Bioorganic & Medicinal Chemistry 16 (2008) 9498–9510

Contents lists available at ScienceDirect

Bioorganic & Medicinal Chemistry

journal homepage: www.elsevier.com/locate/bmc

Synthesis, biological evaluation, and molecular modeling investigation of chiral 2-(4-chloro-phenoxy)-3-phenyl-propanoic acid derivatives with PPARα and PPARγ agonist activity

Giuseppe Fracchiolla [a], Antonio Lavecchia [b,*], Antonio Laghezza [a], Luca Piemontese [a], Raffaella Trisolini [a], Giuseppe Carbonara [a], Paolo Tortorella [a], Ettore Novellino [b], Fulvio Loiodice [a,*]

[a] Dipartimento Farmaco-Chimico, Università degli Studi di Bari, via Orabona 4, 70126 Bari, Italy
[b] Dipartimento di Chimica Farmaceutica e Tossicologica, Università degli Studi di Napoli 'Federico II', via Montesano 49, 80131 Napoli, Italy

ARTICLE INFO

Article history:
Received 16 June 2008
Revised 12 September 2008
Accepted 16 September 2008
Available online 19 September 2008

Keywords:
Chirality
Peroxisome proliferator-activated receptor
Docking
Molecular dynamics
MM–PBSA

ABSTRACT

PPARs are ligand-activated transcription factors that govern lipid and glucose homeostasis and play a central role in cardiovascular disease, obesity, and diabetes. Herein, we present screening results for a series of chiral 2-(4-chloro-phenoxy)-3-phenyl-propanoic acid derivatives, some of which are potent PPARγ agonists as well as PPARα agonists. To investigate the binding modes of the most interesting derivatives into the PPARα and PPARγ binding clefts and evaluate their agonist activity, docking experiments, molecular dynamics simulations, and MM–PBSA analysis were performed.

1. Introduction

Type 2 diabetes accounts for over 90% of the diabetic cases reported in the western world. The global incidence of this disease is estimated to be 150 million people at present and is expected to increase to 220 million people by 2010.[1] This metabolic disorder is characterized by progressive insulin secretory dysfunction and insulin resistance at major target tissues such as skeletal muscle, liver, and adipose tissue, and is usually associated with the so-called metabolic syndrome including dyslipidemia, hypertension, and obesity. Several drugs are currently available for the treatment of Type 2 diabetes including various insulin formulations, sulfonylureas, biguanides, glinides, and α-glucosidase inhibitors. Among the many approaches being evaluated for the discovery of new agents,[2–4] one of the most promising is certainly represented by the exploitation of peroxisome proliferator-activated receptor (PPAR) ligands.

Peroxisome proliferator-activated receptors (PPARs) are ligand-activated transcription factors belonging to the nuclear hormone receptor superfamily.[5] PPARs are activated by a wide range of naturally occurring or metabolized lipids derived from the diet or from intracellular signaling pathways, which include saturated and unsaturated fatty acids and fatty acid derivatives such as prostaglandins and leukotriens.[6,7] Activation of PPARs leads to the formation of heterodimers with retinoid-X receptors (RXRs) forming a complex that interacts with specific DNA response elements within promoter regions of target genes. When activated by agonist ligand binding, this heterodimer complex recruits transcription coactivators and regulates the transcription of genes involved in the control of lipid and carbohydrate metabolism.

There are three PPAR subtypes which are the products of distinct genes and are commonly designated PPARα, PPARγ, and PPARδ. Fibrates are PPARα agonists widely prescribed as hypolipidemic agents to reduce triglycerides while increasing plasma HDL cholesterol.[8] Moreover, they reduce vascular inflammation and thrombogenicity.[9] Thiazolidine-2,4-diones (TZDs or glitazones), on the other hand, are oral anti-diabetic PPARγ agonists which have beneficial effects on glucose homeostasis by increasing insulin sensitivity and glucose disposal and prevent the loss of β cell mass in the pancreas.[10–13] To date, no PPARδ agonist has been fully developed and the clinical potential of targeting this isotype remains to be clearly determined.

Initial strategies were aimed to develop new highly potent specific PPARα or PPARγ agonists. However, combination therapy with drugs acting on both PPAR isotypes may have synergistic and wider therapeutic effects improving both glucose and lipid

* Corresponding authors. Fax: +39 081 678613 (A.L.), +39 080 5442231 (F.L.).
E-mail addresses: lavecchi@unina.it (A. Lavecchia), floiodice@farmchim.uniba.it (F. Loiodice).

0968-0896/$ - see front matter © 2008 Published by Elsevier Ltd.
doi:10.1016/j.bmc.2008.09.045

metabolism of patients suffering from metabolic syndrome and/or Type 2 diabetes. Based on this hypothesis, the concept of identifying ligands that bind and activate both PPARα and PPARγ represents a logical continuation in the field of PPAR research and many groups, in fact, have ongoing research programs to identify more potent and less toxic PPARα/γ dual agonists.

We previously reported the *S*-isomer of compound **1** (Fig. 1) as a promising PPARα/γ dual ligand. Using this compound as the lead structure, we prepared a series of derivatives characterized from: (a) the substitution of the chlorine atom with groups having different electronic and steric properties; (b) the isosteric replacement of the phenolic oxygen with sulfur or amino group, and (c) the lengthening of the methylenic bridge between the chiral carbon and the phenyl ring. These structural modifications led to the identification of some very interesting PPARα/γ dual agonists in which the absolute configuration, also, played a crucial role.[14,15]

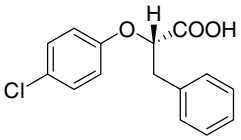

Figure 1. Compound (*S*)-**1** shown to have promising dual agonist activity toward PPARα and PPARγ.

With the aim of improving the potency and efficacy of these compounds, we decided a further investigation of this series taking into account the effects deriving from the introduction of one or more substituents in different positions of both the aromatic rings of the lead compound **1** while maintaining the chlorine atom in the *para* position of the phenoxy moiety. In this paper, therefore, we report the synthesis and PPARα and PPARγ activity of the 2-(4-chloro-phenoxy)-3-phenyl-propanoic acid derivatives displayed in Table 1. The PPARδ activity has not been evaluated given that 2-aryloxy-acetic acids with a bulky substituent situated alpha to the carboxylic group are expected to have very low or no activity on PPARδ.[14,15] Considering the high degree of stereoselectivity shown from the previously reported derivatives of this series of chiral PPARs ligands,[14] the influence of absolute configuration was also taken into account for the compounds esteemed to be more interesting.

The PPARα and PPARγ activity of all derivatives was evaluated by the transactivation assay, a powerful and widely used assay that is generally accepted to correlate well with in vivo activity.

Table 1
Structure and physical properties of compounds **1**–**30**

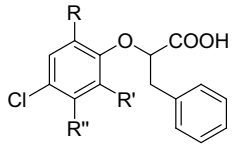

1-10

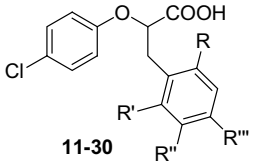

11-30

Compound	R	R′	R″	Formula[a]	Mp (°C)	Recryst. solv.
1[b]	H	H	H	$C_{15}H_{13}ClO_3$	114–115	*n*-Hexane
2	Cl	H	H	$C_{15}H_{12}Cl_2O_3$	98–99	*n*-Hexane
3	Br	H	H	$C_{15}H_{12}BrClO_3$	113–114	*n*-Hexane/$CHCl_3$
4	CH_3	H	H	$C_{16}H_{15}ClO_3$	112–113	*n*-Hexane
5	*n*-Pr	H	H	$C_{18}H_{19}ClO_3$	92–93	*n*-Hexane
6	*n*-Hex	H	H	$C_{21}H_{25}ClO_3$	76–77	*n*-Hexane
7	Ph	H	H	$C_{21}H_{17}ClO_3$	138–139	*n*-Hexane/$CHCl_3$
8	Cl	Cl	H	$C_{15}H_{11}Cl_3O_3$	88–89	*n*-Hexane
9	CH_3	CH_3	H	$C_{17}H_{17}ClO_3$	105–106	*n*-Hexane
10	H	H	Cl	$C_{15}H_{12}Cl_2O_3$	118–119	*n*-Hexane/$CHCl_3$

Compound	R	R′	R″	R‴	Formula[a]	Mp (°C)	Recryst. solv.
11	Cl	H	H	H	$C_{15}H_{12}Cl_2O_3$	111–112	*n*-Hexane
12	Br	H	H	H	$C_{15}H_{12}BrClO_3$	112–113	*n*-Hexane/$CHCl_3$
13	CH_3	H	H	H	$C_{16}H_{15}ClO_3$	84–85	*n*-Hexane
14	*n*-Pr	H	H	H	$C_{18}H_{19}ClO_3$	111–112	*n*-Hexane/$CHCl_3$
15	*n*-Hex	H	H	H	$C_{21}H_{25}ClO_3$	76–78	*n*-Hexane
16	Ph	H	H	H	$C_{21}H_{17}ClO_3$	77–78	*n*-Hexane/$CHCl_3$
17	CF_3	H	H	H	$C_{16}H_{12}ClF_3O_3$	70–71	*n*-Hexane
18	PhO	H	H	H	$C_{21}H_{17}ClO_4$	103–104	*n*-Hexane/$CHCl_3$
19	Cl	Cl	H	H	$C_{15}H_{11}Cl_3O_3$	133–135	*n*-Hexane/$CHCl_3$
20	CH_3	CH_3	H	H	$C_{17}H_{17}ClO_3$	113–115	*n*-Hexane
21[b]	H	H	H	Cl	$C_{15}H_{12}Cl_2O_3$	130–131	*n*-Hexane/$CHCl_3$
22	H	H	H	Br	$C_{15}H_{12}BrClO_3$	87–89	*n*-Hexane/$CHCl_3$
23	H	H	H	CH_3	$C_{16}H_{15}ClO_3$	130–131	*n*-Hexane/$CHCl_3$
24	H	H	H	*n*-Pr	$C_{18}H_{19}ClO_3$	132–133	*n*-Hexane
25	H	H	H	*n*-Hex	$C_{21}H_{25}ClO_3$	87–89	*n*-Hexane
26	H	H	OPh	H	$C_{21}H_{17}ClO_4$	107–108	*n*-Hexane/$CHCl_3$
27	H	H	H	OPh	$C_{21}H_{17}ClO_4$	106–107	*n*-Hexane/$CHCl_3$
(*R*)-**27**	H	H	H	OPh	$C_{21}H_{17}ClO_4$	99–100	*n*-Hexane/$CHCl_3$
(*S*)-**27**	H	H	H	OPh	$C_{21}H_{17}ClO_4$	99–100	*n*-Hexane/$CHCl_3$
(*S*)-**28**	H	H	H	Ph	$C_{21}H_{17}ClO_4$	113–114	*n*-Hexane/$CHCl_3$
(*S*)-**29**	H	H	H	2-Th	$C_{19}H_{17}ClO_3S$	129–130	*n*-Hexane/$CHCl_3$
(*S*)-**30**	H	H	H	CF_3	$C_{16}H_{12}ClF_3O_3$	126–127	*n*-Hexane/$CHCl_3$

[a] Elemental analyses for C, H, and S were within ±0.4% of the theoretical values for the formulas given.
[b] See Ref. 15.

2. Results and discussion

2.1. Chemistry

Racemates **2–4** and **6–10** were prepared as depicted in Scheme 1. The Mitsunobu condensation of ethyl phenyllactate with 4-chlorophenols **2a–4a** and **8a–10a** afforded phenoxyesters **2b–4b** and **8b–10b** which were hydrolyzed to give the desired acids **2–4** and **8–10**. Alternatively, the bromo-derivative **3b** was condensed with *n*-hexyl or phenylboronic acid in Suzuki conditions to give the corresponding intermediates **6c** and **7c** whose hydrolysis afforded acids **6** and **7**, respectively.

A different procedure (Scheme 2) was followed to obtain **5** which was prepared by condensation of 5-chloro-salicylaldehyde with *O*-methanesulfonyl-phenyllactate followed by Wittig reaction with ethyl-triphenylphosphonium bromide, hydrogenation in the presence of Wilkinson catalyst and alkaline hydrolysis.

Racemates **11–13**, **17–23**, **26**, and **27** were prepared by condensation of diethyl 4-chlorophenoxymalonate[16] with benzyl-bromides **11a–13a**, **17a–23a**, **26a**, and **27a** in the presence of NaH (Scheme 3) followed by alkaline hydrolysis and thermal decarboxylation at 160 °C. All the benzyl-bromides were commercially available except for **20a**, **26a**, and **27a** which were prepared from the treatment with PBr_3 of the corresponding benzyl alcohols **20c**, **26c**, and **27c** (Scheme 4). These alcohols, in turn, were obtained by reducing the acids **20b** and **27b** with BMS or the aldehyde **26b** with $NaBH_4$, respectively. The preparation of **14–16**, **24**, and **25**, instead, started from bromo-acids **12** or **22** (Scheme 3) which were esterified, condensed with *n*-propyl, *n*-hexyl, or phenylboronic acid in Suzuki conditions and finally hydrolyzed to give the desired analogues.

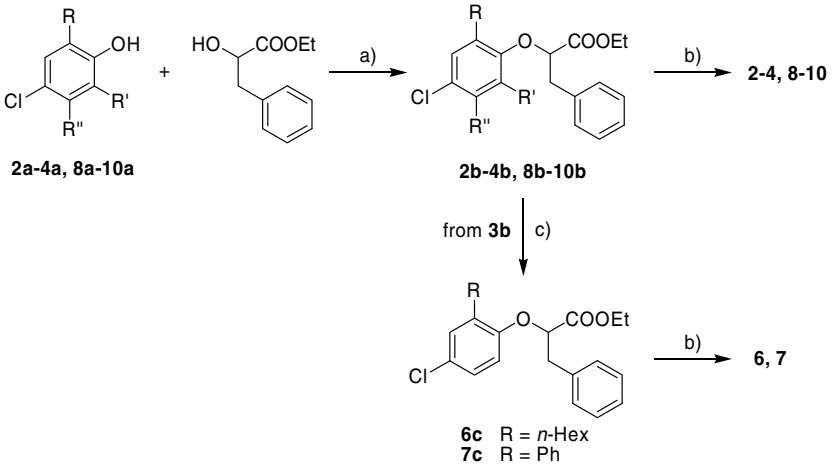

Scheme 1. Reagents and conditions: (a) Ph_3P, DIAD, dry THF; (b) 1 N or 2 N NaOH/THF 1:1; (c) *n*-HexB$(OH)_2$ or PhB$(OH)_2$, Pd$(Ph_3P)_4$, Cs_2CO_3, dry toluene, 95 °C.

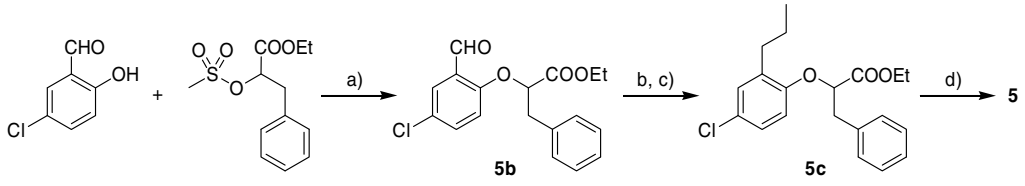

Scheme 2. Reagents and conditions: (a) EtOH, Na, reflux; (b) $(C_2H_5)Ph_3PBr$, DBU, dry CH_3CN; (c) H_2, Wilkinson cat. EtOH, rt; (d) 2 N NaOH/THF 1:1.

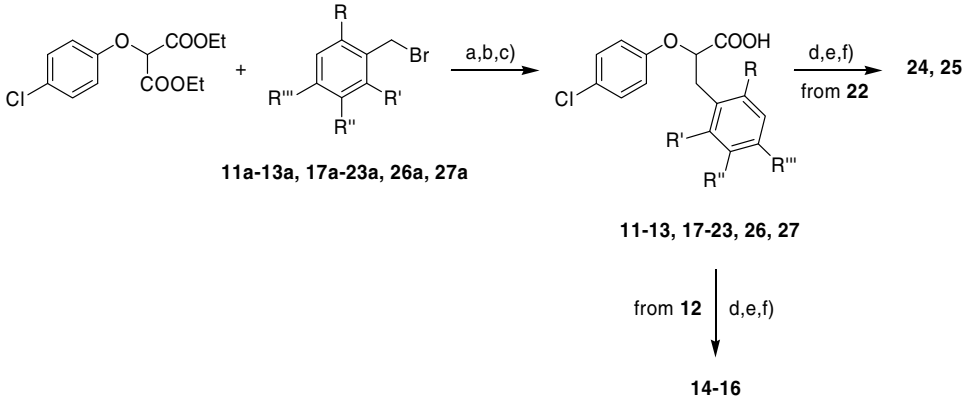

Scheme 3. Reagents and conditions: (a) NaH 95% powder, dry DMF; (b) 1 N NaOH, 95% EtOH; (c) decarboxylation at 160 °C; (d) EtOH, H_2SO_4 cat; (e) *n*-PrB$(OH)_2$, *n*-HexB$(OH)_2$, or PhB$(OH)_2$, Pd$(Ph_3P)_4$, Cs_2CO_3, dry toluene, 95 °C; (f) 2 N NaOH/THF 1:1.

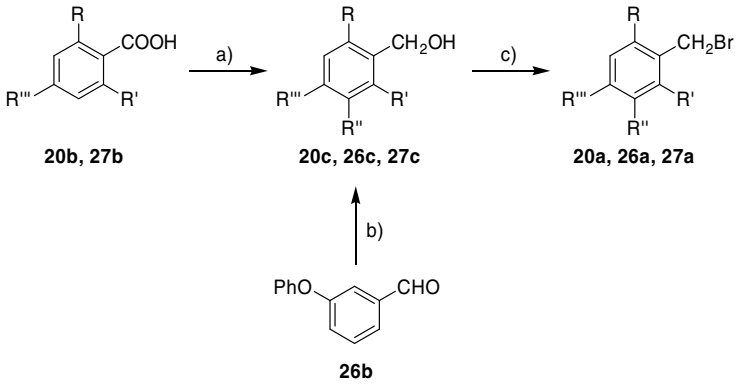

Scheme 4. Reagents and conditions: (a) BMS, dry THF; (b) $NaBH_4$, CH_3OH, 0 °C; (c) PBr_3.

Stereoisomers of compound **27** were obtained by fractional crystallization followed by hydrolysis of the diastereomeric esters through condensation with (*R*)- or (*S*)-pantolactone (Scheme 5).

The absolute configuration of these enantiomers was determined on the basis of circular dichroism analysis; the *S-configuration* was assigned to the dextrorotatory isomer whose CD curve shows a negative Cotton effect around 280 nm and a positive Cotton effect around 235 nm. These effects in CD are also present for the stereochemically ascertained *S*-isomers of **1** and **28** which were used as reference compounds for their structural similarity. The absolute configuration of the former was previously reported,[14] whereas for the latter it was assigned on the basis of the known stereochemical course of its synthetic pathway. Analogues (*S*)-**28** and (*S*)-**29**, in fact, were prepared starting from the commercially available (*R*)-4-nitro-phenylalanine (Scheme 6) which was converted into the corresponding (*R*)-hydroxy-ester **28a** (X = NO_2) through a procedure known to occur with retention of configuration.[17] This intermediate was condensed with 4-chlorophenol under Mitsunobu conditions affording a compound with inverted configuration[18] that, after reduction of nitro- to amino group, underwent a Sandmeyer reaction to give the bromo-derivative **28b**. The Suzuki cross-coupling reaction with phenyl- or 2-thiopheneboronic acid and the final hydrolysis led to the desired acids (*S*)-**28** and (*S*)-**29**, respectively. In the same way, (*R*)-hydroxy-ester **30a** (X = CF_3) was prepared starting from (*R*)-4-trifluoromethylphenylalanine; again, the Mitsunobu condensation with 4-chlorophenol afforded a compound with inverted configuration[18] that, after hydrolysis, led to (*S*)-**30**.

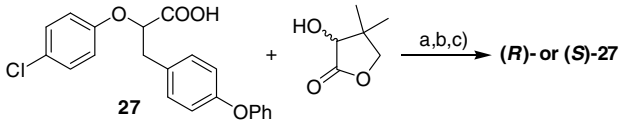

Scheme 5. Reagents and conditions: (a) DCC, DMAP; (b) crystallization from *n*-hexane/CH_2Cl_2; (c) LiOH, 35% H_2O_2, THF/H_2O 4:1.

2.2. PPAR activity

Compounds **2–30** were evaluated for their agonist activity toward the human PPARα (hPPARα) and PPARγ (hPPARγ) subtypes. For this purpose, GAL4-PPAR chimeric receptors were expressed in transiently transfected HepG2 cells according to a previously reported procedure.[19] The results obtained were compared with corresponding data for Wy-14,643 and rosiglitazone used as reference compounds in the PPARα and PPARγ transactivation assays, respectively (Table 2). Maximum obtained fold induction with the reference agonist was defined as 100%.

As shown in Table 2, the introduction of substituents *ortho* to the phenolic oxygen of **1** induced a remarkable decrease of PPAR activity, especially PPARα. Only compounds with a halogen (**2 and 3**) displayed higher potency and similar efficacy on PPARγ compared with **1**. Analogues **4–7**, characterized from the presence of a methyl or bulkier groups, and *ortho*-disubstituted **8**–**9** were practically inactive on both receptors. The placement of the second

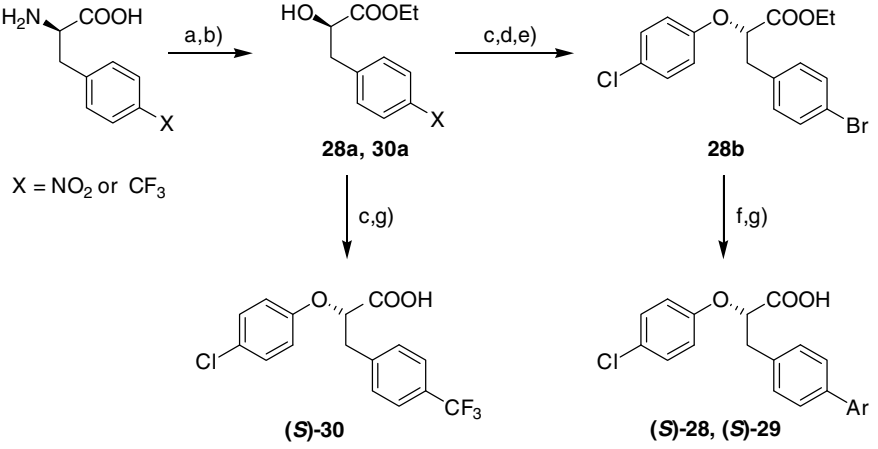

Scheme 6. Reagents and conditions: (a) $NaNO_2$, CH_3COOH/1 N HCl; (b) EtOH, H_2SO_4; (c) 4-chloro-phenol, PPh_3, DIAD, dry toluene; (d) 95% EtOH, CH_3COOH glac., Fe; (e) $NaNO_2$ /H_2O, HCl concd, 48% HBr, CuBr; (f) $PhB(OH)_2$ or 2-thiopheneB$(OH)_2$, $Pd(Ph_3P)_4$, K_2CO_3, dry toluene; (g) 1 N NaOH/THF 1:1.

Table 2
Activity of the tested compounds in cell-based transactivation assay

Compound	PPARα		PPARγ	
	EC_{50} (μM)	Efficacy (%)	EC_{50} (μM)	Efficacy (%)
1	7.94 ± 1.70	82 ± 4	14.46 ± 3.46	48 ± 4
2	n.c.	31 ± 4	2.12 ± 0.59	50 ± 1
3	n.c.	18 ± 2	1.65 ± 0.21	41 ± 4
4	n.c.	34 ± 3	n.c.	34 ± 7
5	n.c.	20 ± 3	n.c.	18 ± 1
6	i.a.	i.a.	i.a.	i.a.
7	i.a.	i.a.	i.a.	i.a.
8	i.a.	i.a.	i.a.	i.a.
9	i.a.	i.a.	i.a.	i.a.
10	2.55 ± 0.07	47 ± 1	4.49 ± 1.29	27 ± 5
11	2.23 ± 0.52	64 ± 6	2.18 ± 0.66	44 ± 1
12	2.48 ± 0.22	61 ± 7	2.25 ± 0.30	57 ± 3
13	8.54 ± 1.92	74 ± 2	9.25 ± 1.48	50 ± 8
14	3.68 ± 0.88	28 ± 3	1.43 ± 0.10	43 ± 3
15	i.a.	i.a.	i.a.	i.a.
16	i.a.	i.a.	i.a.	i.a.
17	4.03 ± 2.50	26 ± 1	2.49 ± 0.13	43 ± 3
18	i.a.	i.a.	1.14 ± 0.65	40 ± 6
19	i.a.	i.a.	i.a.	i.a.
20	i.a.	i.a.	i.a.	i.a.
21	3.16 ± 0.21	77 ± 6	2.23 ± 0.23	49 ± 1
22	2.07 ± 0.47	76 ± 6	1.10 ± 0.06	46 ± 3
23	4.36 ± 0.01	74 ± 6	2.81 ± 0.44	53 ± 8
24	1.39 ± 0.26	48 ± 0	0.35 ± 0.21	39 ± 5
25	n.c.	31 ± 4	0.45 ± 0.02	56 ± 8
26	3.06 ± 0.99	42 ± 0	0.24 ± 0.16	57 ± 4
27	1.06 ± 0.07	22 ± 2	0.064 ± 0.008	58 ± 9
(*R*)-**27**	11.30 ± 5.23	25 ± 4	0.70 ± 0.02	15 ± 3
(*S*)-**27**	0.87 ± 0.19	32 ± 1	0.027 ± 0.003	68 ± 6
(*S*)-**28**	1.12 ± 0.08	40 ± 2	0.049 ± 0.003	70 ± 6
(*S*)-**29**	0.59 ± 0.02	46 ± 1	0.065 ± 0.004	71 ± 5
(*S*)-**30**	3.65 ± 1.23	60 ± 13	0.42 ± 0.02	69 ± 11
Wy-14,643	1.60 ± 0.30	100 ± 9	i.a.	i.a.
Rosiglitazone	i.a.	i.a.	0.039 ± 0.003	100 ± 9

i.a., inactive at tested concentrations. Efficacy values were calculated as percentage of the maximum obtained fold induction with the reference compounds (Wy-14,643 for PPARα; rosiglitazone for PPARγ).
n.c., not computable; the activity, in fact, increases with increasing concentrations up to 10 μM above which the activity begins to decrease.

chlorine atom *meta* to the phenolic oxygen of **1** afforded compound **10** which turned out to be more potent on both PPARα and PPARγ, but significantly less efficacious.

When the *ortho* substitution was carried out on the aromatic ring of the benzylic moiety of **1**, a similar behavior was observed. Bulky groups (**15** and **16**) or *ortho*-disubstitution (**19** and **20**) provided compounds completely inactive; in this case, the presence of a halogen (**11** and **12**) increased the potency on both receptors with almost no influence on efficacy. The introduction of a methyl (**13**) kept the activity basically unchanged with a gain only on PPARγ potency. Analogues **14** and **17**, having a trifluoromethyl and an isopropyl group, respectively, exhibited higher potency on both receptor subtypes with reduced efficacy on PPARα but unaltered on PPARγ. The *ortho*-phenoxyl derivative **18**, as for phenyl analog **16**, was completely devoid of activity on PPARα, but ten times more potent than **1** on PPARγ. When this substituent was moved to *meta* and *para* positions of the benzylic ring, the so obtained compounds **26** and **27** displayed a remarkable increase on PPARγ potency, about one and two orders of magnitude, respectively, up to values comparable to that of rosiglitazone even though less effective. Further, these two derivatives revealed a significative PPARα agonist activity. Similarly, the displacement of other substituents from *ortho* to *para* position led to more potent and effective PPARα and PPARγ agonists (**21–24**); only the *para*-hexyl derivative **25** was almost inactive on PPARα isoform. To evaluate the influence of the absolute configuration on PPAR activity in this series of compounds, we prepared the optical isomers of the potent PPARγ agonist **27**. Also in this case, as previously reported for other 2-aryloxy-3-phenyl-propanoic acids,[14] the *S*-isomer confirmed to be more active with a potency about 10 and 30 times higher than that of *R*-isomer on PPARα and PPARγ, respectively. At this point, on the analogy of the type of substitution previously carried out on the aryloxy moiety of 2-aryloxy-3-phenyl-propanoic acids which had afforded very interesting dual PPARα/PPARγ agonists,[14] we introduced the same functional groups on the benzylic nucleus of **27** inserting phenyl, 2-thienyl or trifluoromethyl in place of the phenoxy group. The so obtained derivatives **28–30** were prepared only as *S*-isomers and displayed to be all very potent PPARγ agonists with good potency and moderate efficacy on PPARα too.

2.3. Molecular modeling

To help interpretation of SAR data and to increase our understanding of the main binding interactions at the PPARα and PPARγ binding sites, docking experiments, and molecular dynamics (MD) simulations combined with MM–PBSA (molecular mechanics and Poisson–Boltzmann surface area) technique were performed on the most active dual PPARα/PPARγ agonists (*S*)-**27** and (*S*)-**29**, as well as the less potent (*S*)-**30**. To this end, the crystal structures of the human PPARα (hPPARα) complexed with bound agonist GW409544 (PDB code: 1K7L)[20] and the human PPARγ (hPPARγ) in complex with the agonist rosiglitazone (PDB code: 2PRG)[21] were employed. The ligand–receptor complexes were predicted through the automated docking software GOLD 3.1,[22,23] which in several studies was shown to yield better performances compared to other similar programs.[24–27]

Docking of (*S*)-**27** into the hPPARα crystal structure revealed a very clear preference for two prevailing poses in the binding site; these are designated binding orientations A and B, as shown in Figure 2. Interestingly, both results were located in the binding pocket and occupied the same spatial position as the crystallized agonist GW409544. The top-ranking result (GOLD fitness score = 16.5 kcal mol^{-1}), corresponding to orientation A, had its carboxylate group H-bonded with S280, Y314, and Y464 side chains, while the *p*-chlorophenoxy and *p*-phenoxybenzyl groups were hosted in two hydrophobic pockets, respectively (Fig. 2a). In particular, the *p*-chlorophenoxy ring lodged in a hydrophobic cavity formed by T279, I317, F318, and L321 side chains. The L321 side chain appeared in a suitable position to make lipophilic interactions with the *p*-chlorine atom of (*S*)-**27**. The *p*-phenoxybenzyl moiety pointed to a large hydrophobic cleft lined by residues I272, F273, L344, L347, F351, I354, M355, and I447. F273 and F351 formed face-on-face and face-edge-face aromatic-stacking interactions with the two aromatic rings of the *p*-phenoxybenzyl moiety of the ligand, respectively. Notably, the C276 side chain was in close contact with both aromatic rings of the benzyl and *p*-chlorophenoxy groups of the ligand, making additional hydrophobic interactions. Interestingly, the second-ranking result (GOLD fitness score = 15.5 kcal mol^{-1}), which corresponds to orientation B, resembled the top one, except for the *p*-chlorophenoxy and *p*-phenoxybenzyl moieties, which occupied the two above cited hydrophobic pockets in opposite fashion (Fig. 2b). It is to note that in this binding orientation, the *p*-chlorophenoxylic oxygen of (*S*)-**27** established an additional H-bond with the H440 $N^{\varepsilon 2}$ atom.

As GOLD treats the ligand in a flexible way allowing receptor flexibility only to a limited extent, an exhaustive protocol of MD simulation was applied, both to relax the ligand/hPPARα complexes and to obtain a better understanding of the energetic contributions to the binding. We hypothesized that this procedure might eventually lead us to find more reliable results about the preferred orientation of the ligand into hPPARα. For this purpose, 3 ns of MD simulations were carried out on the complexes formed between hPPARα and the two prevailing docking orientations A and B found

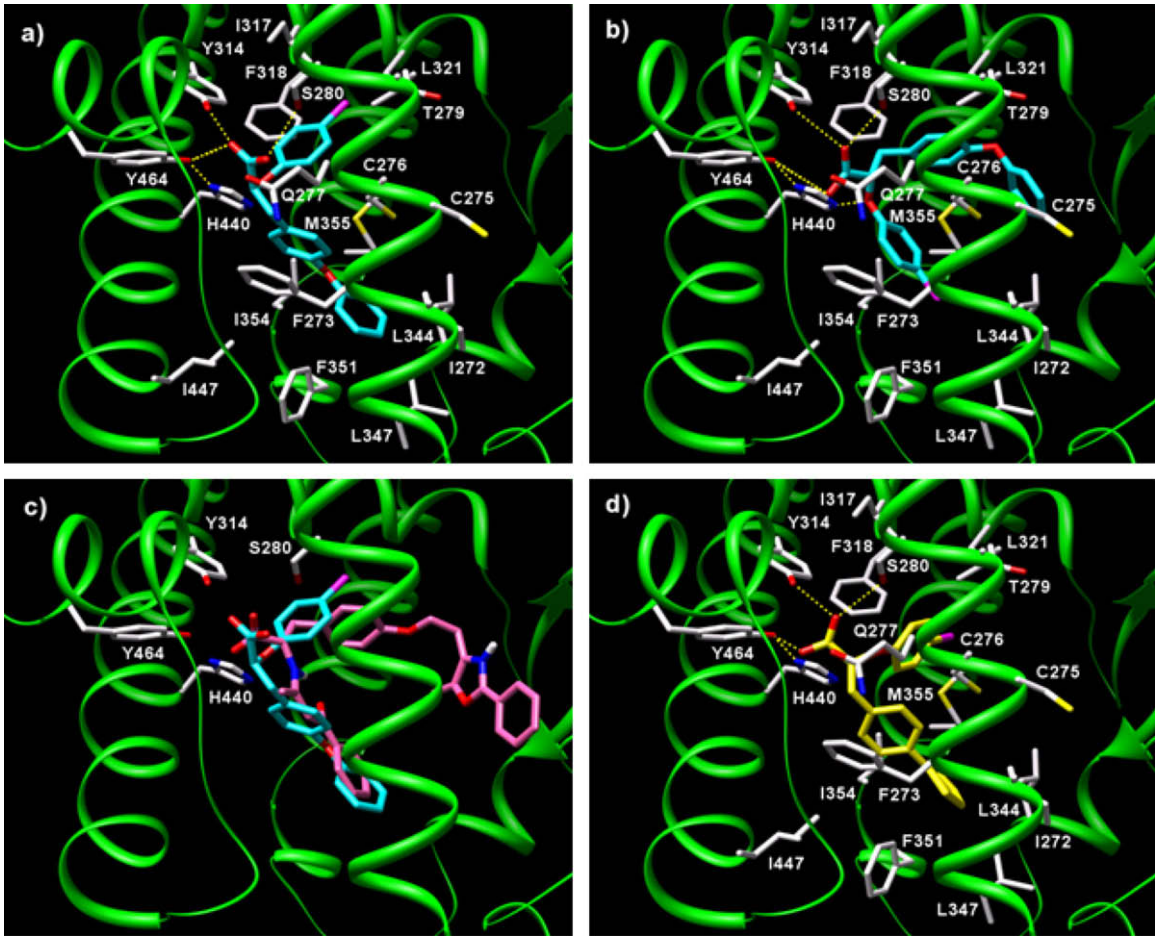

Figure 2. Compounds (*S*)-**27** (cyan) and (*S*)-**29** (yellow) docked into the hPPARα binding site represented as a green ribbon model. (a) Binding mode A of (*S*)-**27**. (b) Binding mode B of (*S*)-**27**. (c) Superimposition of the binding mode A of (*S*)-**27** on the PPARα-bound conformation of GW409544 (pink). (d) Binding mode of (*S*)-**29**. Only amino acids located within 4 Å of the bound ligand are displayed (white) and labeled. Hydrogen bonds discussed in the text are depicted as dashed yellow lines.

for compound (*S*)-**27**. The trajectory was subsequently analyzed by using the MM–PBSA method.[28–30] This approach considers the contribution of the electrostatic and deformation energy terms as well as the desolvation energy.

MD trajectories (data not shown) suggested that hPPARα produced stable complexes with both orientation A and B of (*S*)-**27**, as confirmed by their low rmsd fluctuations (1.5 Å and 1.8 Å, respectively). The ligand interactions observed in the starting structures were also maintained throughout the MD simulation. Moreover, when the ligand was in the binding orientation A, the MD simulation model allowed the formation of an additional tight H-bond between its carboxylate group and the Q277 $N^{\varepsilon 2}$ atom. This interaction was observed in 79% of the snapshots taken during the MD simulation.

MM–PBSA using the single trajectory method was performed to calculate binding free energies (ΔG_{bind}). Three hundred snapshots were taken every 10 ps from the MD trajectories for analysis of the binding free energy. Table 3 reports the MM–PBSA results calculated for (*S*)-**27** (A and B conformations) into hPPARα. Considering the impracticality of normal mode calculations for the large size of these complexes and the uncertainties in the entropic calculation, entropic effects of the solute were not explicitly taken into account. For compounds with similar structures, the entropy contribution can be omitted if one is only interested in the relative order of binding affinities.[31] The ΔG_{bind} of binding mode A was −48.84 kcal mol^{-1}, about 6.5 kcal mol^{-1} more negative than the second best binding mode (orientation B, ΔG_{bind} = −42.37 kcal mol^{-1}), suggesting that the (*S*)-**27**/hPPARα complex had a better interaction energy when the ligand was positioned into the A orientation. The gas-phase electrostatic values (ΔE_{ele}) of the two complexes showed that the electrostatic interactions were in favor of the binding. In particular, the ΔE_{ele} value of orientation B was smaller than that of orientation A, indicating that the electrostatic interactions favored the orientation A more than the corresponding orientation B. This was in agreement with the H-bond analysis, showing that only orientation A formed an additional H-bond with

Table 3
Relative binding free energies (ΔG_{bind}) of two binding modes A and B of (*S*)-**27** in complex with hPPARα[a]

Binding orientation	ΔE_{ele}	ΔE_{vdw}	ΔE_{gas}	ΔE_{sur}	ΔE_{cal}	ΔE_{pbsol}	ΔE_{pbele}	ΔG_{bind}[b]
A	−49.66	−47.01	−96.67	−6.32	54.15	47.83	4.49	−48.84
B	−39.66	−44.93	−84.59	−6.58	48.80	42.22	9.14	−42.37

[a] All energies are given in kcal mol^{-1}, and the symbols are explained in the text.
[b] Calculation of ΔG_{bind} does not explicitly consider entropy contributions.

Q277. The van der Waals interaction energies (ΔE_{vdw}) of the two complexes also contributed favorably to the binding. The ΔE_{vdw} value of orientation A was a little higher than that of orientation B, because when the ligand was in A orientation fitted more snugly within the binding cavity and had a tighter binding to hPPARα, adding non-polar packing in the binding site to a much deeper extent. The energy difference ΔE_{vdw} between these two complexes was not large, which might indicate that the van der Waals interactions are not an important factor for the binding affinity difference between orientations A and B of the ligand. Figure 2c shows a superimposition of orientation A of (*S*)-**27** on the PPARα-bound conformation of GW409544. Interestingly, it can be noted that the ligand mimics one of the two branches of GW409544.

A convergent binding mode was largely adopted when (*S*)-**29** was docked into the hPPARα binding cleft (GOLD fitness score = 14.6 kcal mol^{-1}). As depicted in Figure 2d, the associated binding mode closely resembled the above-described binding orientation A of (*S*)-**27** with the carboxylate group still interacting with S280, Y314, and Y464 and the *p*-chlorophenoxy and *p*-thiophenebenzyl moieties placed in the two above mentioned hydrophobic pockets. As regards compound (*S*)-**30**, results from GOLD runs suggested multiple docking poses characterized by quite diverse binding modes but comparable fitness scores (in the range 12.2–14.1 kcal mol^{-1}). Inspection of the top-ranking docking solutions revealed that no H-bonds were formed between the carboxylate group of (*S*)-**30** and the critical residues S280, Y314, and Y464 of hPPARα. The poor docking run convergence toward a single binding mode, the lower estimated GOLD fitness score and the absence of H-bonds with S280, Y314, and Y464 would suggest that compound (*S*)-**30** forms a less stable complex with hPPARα, in agreement with the SAR data showing that this ligand has lower potency on hPPARα (EC_{50} = 3.65 μM).

To rationalize the high potency but partial PPARγ agonist activity of (*S*)-**27**, (*S*)-**29**, and (*S*)-**30**, docking experiments into the hPPARγ receptor binding domain were carried out.[21] GOLD successfully predicted a distinct solution for (*S*)-**27** (GOLD fitness score = 15.5 kcal mol^{-1}). In the predicted binding orientation, the carboxylate group made a H-bond with Y327 and S289, whereas the *p*-chlorophenoxy and the *p*-phenoxybenzyl moieties were lodged in two hydrophobic pockets (Fig. 3a). In particular, the *p*-chlorophenoxy ring contacted residues F282, Q286, F363, H449, L453, L465, L469, and Y473, whereas the *p*-phenoxybenzyl group interacted with I326, L330, A292, I296, M329, and L333. A cation–π interaction was also observed between the phenoxy aromatic ring of the *p*-phenoxybenzyl moiety and the R288 guanidinium group. A binding mode very similar was also found for compound (*S*)-**29** (GOLD fitness score = 16.0 kcal mol^{-1}), in which all the ligand/receptor interactions above cited for (*S*)-**27** were preserved (Fig. 3b). As regards (*S*)-**30**, a slight different binding pose was found (GOLD fitness score = 14.3 kcal mol^{-1}). In the predicted

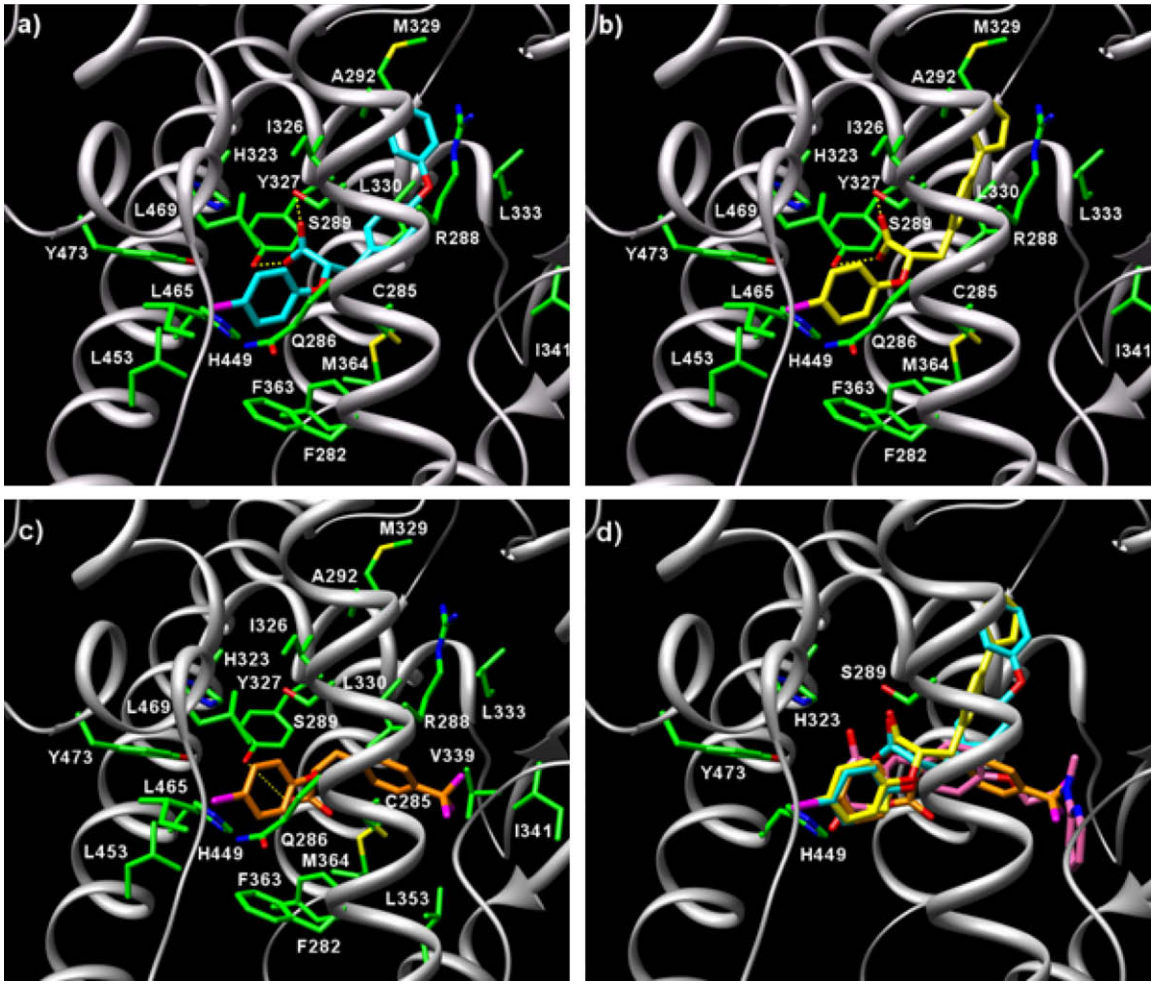

Figure 3. Compounds (a) (*S*)-**27** (cyan), (b) (*S*)-**29** (yellow), and (c) (*S*)-**30** (orange) docked into the hPPARγ binding site represented as a gray ribbon model. (d) Superimposition of the binding mode of (*S*)-**27**, (*S*)-**29**, and (*S*)-**30** on the PPARγ-bound conformation of rosiglitazone (pink). Only amino acids located within 4 Å of the bound ligand are displayed (green) and labeled. Hydrogen bonds discussed in the text are depicted as dashed yellow lines.

binding mode, the carboxylate group of the ligand, differently from (*S*)-**27** and (*S*)-**29**, formed only a H-bond with Y327, whereas the *p*-trifluoromethylbenzyl moiety extended toward the opposite side of the pocket around residues C285, L330, V339, I341, L353, and M364, filling the cavity occupied by the pyridine ring-containing tail of rosiglitazone (see Fig. 3d).

Figure 3d depicts the superimposition of the docked orientation of (*S*)-**27**, (*S*)-**29**, and (*S*)-**30** on the PPARγ-bound conformation of rosiglitazone. As one can see, the binding orientation of (*S*)-**27** and (*S*)-**29** was somewhat different from that of the PPARγ-bound conformation of rosiglitazone, whereas that of (*S*)-**30** was very similar. The thiazolidinedione group of rosiglitazone stretched deep into the left stem of the PPARγ binding cavity and interacted with the AF-2 Y473 of PPARγ, which is known to be important in coactivator binding. The carboxylate group of (*S*)-**27** and (*S*)-**29** was yet situated in the vicinity of the rosiglitazone thiazolidinedione group, while the *p*-phenoxy or *p*-thiophenebenzyl moieties were moved away from the pyridine ring-containing tail of rosiglitazone, stretching deep into the upper part of cavity. Many reports have suggested that the interactions of a ligand with S289, H323, Y473, and H449 are important for the activities of PPARγ agonists, as this H-bonding network could stabilize the AF-2 helix in a conformation which favors the binding of coactivators to PPARγ and, consequently, enhances their recruitment.[21,32] In contrast, in the (*S*)-**27**/PPARγ, (*S*)-**29**/PPARγ, and (*S*)-**30**/PPARγ complexes, the carboxylate group of the ligands was too away from the AF-2 helix and subsequently resulted in the loss of some H-bonds with the key residues of PPARγ. Only the H-bond with S289 was conserved by compounds (*S*)-**27** and (*S*)-**29**. Therefore, the absence of these critical H-bonding interactions with the protein might provide the structural basis for the much weaker transactivation activity of these compounds for PPARγ as compared with rosiglitazone.

In conclusion, we prepared and tested a new series of chiral 2-(4-chloro-phenoxy)-3-phenyl-propanoic acid derivatives, some of which were potent agonists of PPARγ as well as PPARα agonists. Docking experiments and MD simulations combined with MM–PBSA technique were performed on the most interesting derivatives to help interpretation of SAR data and to increase our understanding of the main binding interactions at the receptors binding sites.

3. Experimental

3.1. Biological methods

Medium, other cell culture reagents, and Wy-14,643 were purchased from Sigma (Milan, Italy). BRL 49653 (rosiglitazone) was obtained by Hefei Scenery Chemical Co. (Hefei, Anhui, Popular Republic of China).

3.2. Plasmids

The expression vectors expressing the chimeric receptors containing the yeast GAL4-DNA binding domain fused to the human PPARα or PPARγ ligand binding domain (LBD) and the reporter plasmid for these GAL4 chimeric receptors (pGAL5TKpGL3) containing five repeats of the GAL4 response elements upstream of a minimal thymidine kinase promoter that is adjacent to the luciferase gene were described previously.[33]

3.3. Cell culture and transfections

Human hepatoblastoma cell line HepG2 (Interlab Cell Line Collection, Genoa, Italy) was cultured in minimum essential medium (MEM) containing 10% of heat-inactivated fetal bovine serum, 100 U penicillin G mL^{-1} and 100 μg streptomycin sulfate mL^{-1} at 37 °C in a humidified atmosphere of 5% CO_2. For transactivation assays 10^5 cells per well were seeded in a 24-well plate in triplicate and transfections were performed after 24 h, with CAPHOS® (Sigma, Milan, Italy), a calcium-phosphate method, according to the manufacturer's guidelines. Cells were transfected with expression plasmids encoding the fusion protein GAL4-PPARα LBD or GAL4-PPARγ LBD (30 ng), pGAL5TKpGL3 (100 ng), and pCMVβgal (250 ng). Four hours after transfection, cells were treated for 20 h with the indicated ligands. Luciferase activity in cell extracts was then determined by a luminometer (VICTOR^{3}V Multilabel Reader, Perkin-Elmer). β-Galactosidase activity was determined using β-D-galactopyranoside (Sigma, Milan, Italy) as described previously.[34] All transfection experiments were repeated at least twice.

3.4. General procedures

Column chromatography was performed on ICN silica gel 60 Å (63–200 μm) as a stationary phase. Melting points were determined in open capillaries on a Gallenkamp electrothermal apparatus and are uncorrected. Mass spectra were recorded with a HP GC/MS 6890-5973 MSD spectrometer, electron impact 70 eV, equipped with HP chemstation. ^{1}H NMR spectra were recorded in $CDCl_3$ (the use of DMSO-d_6 as a solvent is specified) on a Varian-Mercury 300 (300 MHz) spectrometer at room temperature (20 °C). Chemical shifts are expressed as parts per million (δ). For optical isomers, MS and ^{1}H NMR spectra are reported only for the racemate or one of the two enantiomers. Microanalyses of solid compounds were carried out with an Eurovector Euro EA 3000 model analyzer; the analytical results are within ±0.4% of theoretical values. Optical rotations were measured with a Perkin-Elmer 341 polarimeter at room temperature (20 °C): concentrations are expressed as g(100 mL)$^{-1}$. The CD curves were registered on a J-810 model JASCO spectropolarimeter. The enantiomeric excesses of acids were determined by HPLC analysis of their methyl esters, obtained by reaction with a solution of diazomethane in Et_2O, on Chiralcel OD or AD columns (4.6 mm id × 250 mm, Daicel Chemical Industries, Ltd, Tokyo, Japan). For this purpose, small amounts of the *R*-enantiomers of **28–30** were also prepared, in particular (*R*)-**28** and (*R*)-**29** were prepared starting from the commercially available L-(4-iodo)phenylalanine, so as to avoid Steps (d and e) of Scheme 6. Analytical liquid chromatography was performed on a PE chromatograph equipped with a Rheodyne 7725i model injector, a 785A model UV/Vis detector, a series 200 model pump and NCI 900 model interface. Chemicals were obtained from Aldrich (Milan, Italy), Lancaster (Milan, Italy), or Acros (Milan, Italy) and were used without any further purification.

4. Chemistry

4.1. Preparation of 2b–4b and 8b–10b: General procedure (Scheme 1)

A solution of diisopropylazodicarboxylate (DIAD, 10 mmol) in dry THF (15 mL) was added dropwise to an ice-bath cooled mixture of ethyl phenyllactate (10 mmol), the suitable substituted phenol (**2a–4a**, **8a–10a**, 10 mmol), and triphenylphosphine (10 mmol) in dry THF (45 mL). The reaction mixture was stirred at room temperature overnight, under N_2 atmosphere. The solvent was evaporated in vacuo and a mixture of Et_2O/*n*-hexane (40 mL, 1:1) was added to the residue. The resulting precipitate was filtered off and the filtrate was evaporated to dryness. The residue was chromatographed on silica gel column (petroleum ether/ethyl acetate 95:5 as eluent), affording the desired compounds.

4.2. Preparation of 6c and 7c (Scheme 1)

n-Hexylboronic acid or phenylboronic acid (3.64 mmol) and Cs_2CO_3 (2.73 mmol) were added, under N_2 atmosphere, to a stirred solution of **3b** (1.82 mmol) in dry toluene (35 mL); after 0.5 h, $Pd(Ph_3P)_4$ (0.055 mmol) was added to the mixture. The reaction mixture was stirred overnight at 95 °C and then quenched with 1 N HCl (7.5 mL) and ethyl acetate (7.5 mL). The suspension was filtered through a Celite pad to remove the catalyst and the filtrate was washed with $NaHCO_3$ saturated solution and brine. After drying over Na_2SO_4, the solvent was evaporated to dryness obtaining a dark oil residue which was chromatographed on silica gel column (petroleum ether/ethyl acetate 98:2 or 95:5 as eluent, respectively), affording the desired compounds as yellow oils.

4.3. Ethyl 2-methanesulfonyloxy-3-phenylpropanoate (Scheme 2)

A solution of methanesulfonyl chloride (0.651 g, 5.61 mmol) in anhydrous CH_2Cl_2 (22 mL) was added dropwise during 10 min to a stirred and ice-bath cooled solution of ethyl phenyllactate (1.001 g, 5.11 mmol). The reaction mixture was stirred at 0 °C for 4 h, then was carefully poured into ice-water and the organic layer was separated and washed with cool 10% HCl followed by brine, $NaHCO_3$ saturated solution, and brine. After drying over Na_2SO_4, the solvent was evaporated to dryness affording a pale yellow oil (1.275 g, 92% yield) which was used for the next step without any further purification.

4.4. Ethyl 2-(2-formyl-4-chloro-phenoxy)-3-phenylpropanoate (5b, Scheme 2)

An abs EtOH (120 mL) solution of ethyl 2-methanesulfonyloxy-3-phenylpropanoate (3.681 g, 13.51 mmol) and sodium 4-chloro-2-formyl-phenate (3.118 g, 17.01 mmol), prepared from equivalent amounts of the corresponding phenol and sodium in abs EtOH (30 mL), was stirred and heated under reflux for 17 h. The solvent was removed under reduced pressure and the residue dissolved in ethyl acetate. The organic phase was washed twice with brine, 2 N NaOH and brine, then was dried over Na_2SO_4, and filtered. The solvent was evaporated to dryness affording a dark oil (4.275 g) which was chromatographed on silica gel column (petroleum ether/ethyl acetate 95:5 as eluent), affording the title compound as a yellow oil (2.112 g, 38% yield).

4.5. Ethyl 2-(2-*n*-propyl-4-chloro-phenoxy)-3-phenylpropanoate (5c, Scheme 2)

A solution of ethyl 2-(2-formyl-4-chloro-phenoxy)-3-phenylpropanoate (0.801 g, 2.41 mmol) in dry CH_3CN (20 mL) was carefully added, under N_2 atmosphere and during 0.5 h, to a stirred solution of (ethyl)triphenylphosphonium bromide (1.893 g, 5.10 mmol) in dry CH_3CN (15 mL). After 0.5 h a solution of DBU (0.807 g, 5.30 mmol) in dry CH_3CN (15 mL) was added to the mixture. The reaction mixture was stirred and heated under reflux for 18 h, the solvent was removed under reduced pressure and the residue dissolved in ethyl acetate. The organic phase was washed with NH_4Cl saturated solution and twice with brine, then was dried over Na_2SO_4, and filtered. The solvent was evaporated to dryness affording a yellow oil (1.528 g) which was chromatographed on silica gel column (petroleum ether/ethyl acetate 95:5 as eluent). The oily mixture of the two propylen stereoisomers so obtained (0.401 g) was dissolved in abs EtOH (90 mL) and stirred at rt under a hydrogen atmosphere (5 atm) in the presence of Wilkinson catalyst (0.062 g). After 9 h the suspension was filtered through a Celite pad to remove the catalyst and the filtrate was concentrated under reduced pressure to give a brown solid (0.421 g) which was chromatographed on silica gel column (Et_2O/CH_2Cl_2 90:10 as eluent), affording the title compound as a colorless oil (0.345 g, 86% yield).

4.6. Preparation of acids 2–10, 14–16, 24, 25, and (*S*)-28–30: General procedure (Schemes 1–3 and 6)

A solution of the corresponding ethyl ester (5 mmol) in THF (30 mL) and 1 N NaOH (30 mL) was stirred at room temperature for 4–6 h. For the acids **5–7**, **14–16**, **24**, and **25**, 2 N NaOH (30 mL) was used, and the reaction was stirred for 20–24 h. The organic layer was removed under reduced pressure and the aqueous phase was acidified with 6 N HCl and extracted with Et_2O or ethyl acetate. The combined organic layers were dried over Na_2SO_4 and evaporated to dryness affording the final acids in quantitative yields as white solids which were recrystallized from the solvent described in Table 1.

4.7. Preparation of diethyl 2-(4-chloro-phenoxy)-2-benzylmalonates (Scheme 3, Step a): General procedure

A solution of diethyl 2-(4-chloro-phenoxy)malonate[16] (10 mmol) in dry DMF (25 mL) was added dropwise to a suspension of NaH (95% powder, 18 mmol) in dry DMF (20 mL) at 0 °C. After stirring at room temperature for 20 min, a solution of the suitable benzylbromide (**11a–13a**, **17a–23a**, **26a**, and **27a**) (12 mmol) in dry DMF (15 mL) was added dropwise and the resulting reaction mixture stirred at 60 °C for 15–20 h. The solvent was removed under reduced pressure and the residue poured into water and extracted with diethyl ether. The organic layer was washed with saturated ammonium chloride solution, dried over Na_2SO_4, and the solvent evaporated in vacuo to give an oily residue which was chromatographed on silica gel column (petroleum ether/ethyl acetate 90:10 as eluent). The title compounds were obtained as pale yellow oils in 37–98% yields.

4.8. Preparation of acids 11–13, 17–23, 26, and 27 (Scheme 3): General procedure

The suitable diethyl malonate (3 mmol), obtained from the reaction described above, was refluxed under stirring with 1 N NaOH (3 mL) in 95% EtOH (12 mL) for 4–6 h. The organic solvent was distilled off under reduced pressure and the remaining aqueous phase washed with Et_2O, acidified to pH 2 with 6 N HCl and extracted with Et_2O. The combined organic extracts were dried over Na_2SO_4 and the solvent removed under reduced pressure. The resulting products were heated at 160 °C for 2 h affording the desired acids in quantitative yields as white solids which were recrystallized from the solvent described in Table 1.

4.9. Preparation of the ethyl esters of 12 and 22 (Scheme 3, Step d)

A solution of **12** or **22** (2 mmol) in abs EtOH (50 mL) was added of a catalytic amount of concd H_2SO_4 and refluxed with stirring for 4 h. The EtOH was distilled off under reduced pressure. The residue was dissolved in ethyl acetate, which was washed with $NaHCO_3$ and brine, then dried over Na_2SO_4, and the solvent removed under reduced pressure affording the title compounds in quantitative yield as pale yellow solids.

4.10. Preparation of the ethyl esters of 14–16, 24, and 25 (Scheme 3, Step e)

These compounds were prepared as reported for **6c** and **7c** starting from the ethyl esters of **12** (for **14–16**) or **22** (for **24** and

25), described above, with the appropriate boronic acid, Cs_2CO_3 and $Pd(Ph_3P)_4$ in anhydrous toluene at 95 °C. The purification was carried out by column chromatography on silica gel using petroleum ether/ethyl acetate 80:20 as eluent.

4.11. Preparation of benzyl alcohols 20c and 27c (Scheme 4)

Borane-methyl sulfide complex (BMS, 45 mmol) was carefully added dropwise, under N_2 atmosphere, to a stirred and cooled to 0 °C solution of commercially available benzoic acid derivatives **20b** or **27b** (15 mmol) in anhydrous THF (70 mL). The reaction mixture was stirred for 15 h at rt, cooled to 0 °C and carefully added of CH_3OH (30 mL, 0.5 h) dropwise to destroy the boran complex excess. After distilling off the organic solvents, the mixture was dissolved in Et_2O and the resulting solution was washed with 2 N NaOH and brine. The organic layer was dried over Na_2SO_4 and filtered. Evaporation of the solvent in vacuo afforded the desired compound as colorless oils in quantitative yield. These compounds were used in the next step without any further purification.

4.12. 3-Phenoxybenzyl alcohol (26c, Scheme 4)

$NaBH_4$ (7.21 mmol) was carefully added, to a stirred and cooled to 0 °C solution of commercially available aldehyde **26b** (5.53 mmol) in CH_3OH (40 mL) and the reaction mixture was stirred for 15 min at 0 °C. After distilling off the organic solvent, the mixture was added of H_2O and extracted with ethylacetate. The combined organic phase was washed with 2 N NaOH and brine. The organic layer was dried over Na_2SO_4 and filtered. Evaporation of the solvent in vacuo afforded the desired compound as a pale yellow oil in 63% yield.

4.13. Preparation of benzyl-bromides 20a, 26a, and 27a (Scheme 4)

PBr_3 (11 mmol) was carefully added to the suitable benzyl alcohol (**20c, 26c, and 27c**) (10 mmol) at 0 °C. The reaction mixture was stirred for 1–2 h at 0 °C and 4–8 h at rt then poured into ice and extracted with Et_2O. The organic layer was washed with brine, dried over Na_2SO_4, and the solvent evaporated in vacuo affording the title compounds as pale yellow oils in quantitative yields. These compounds were used in the next step without any further purification.

4.14. Preparation of (*R*)- or (*S*)-pantolactone esters of 27 (Scheme 5)

(*R*)-Pantolactone (10 mmol), dimethylaminopyridine (DMAP; 0.1 mmol), and 1,3-dicyclohexylcarbodiimide (DCC; 10 mmol) were added, under N_2 atmosphere, to a stirred solution of the racemic acid **27** (10 mmol) in anhydrous THF (40 mL). The reaction mixture was stirred at room temperature for 24 h, afterward the precipitate was filtered off and the organic phase was evaporated to dryness, dissolved in ethyl acetate (50 mL), and washed twice with H_2O, 3 N HCl, and brine. The organic layer was dried over Na_2SO_4 and evaporated to dryness affording a yellow oil. The mixture of the (*R*,*R*)-and (*S*,*R*)-diastereomeric esters was obtained, as white solid, by column chromatography on silica gel using petroleum ether/ethyl acetate 80:20 as eluent. This mixture was recrystallized twice with CH_2Cl_2/*n*-hexane affording the (*R*,*R*)-diastereomer in 25% overall yield. The mother liquors containing an enriched mixture in the (*S*,*R*)-diastereomer were hydrolyzed in alkaline medium affording a mixture of the acid enantiomers, which was condensed with (*S*)-pantolactone and chromatographed as reported above. Then the mixture of diastereomers was recrystallized twice with CH_2Cl_2/*n*-hexane to obtain the (*S*,*S*)-diastereomer in 23% overall yield.

4.15. Preparation of (*S*)- and (*R*)-27 (Scheme 5)

To a stirred and cooled to 0 °C suspension of the suitable pantolactone ester (0.66 mmol) in THF/H_2O (4:1, 12.5 mL) were added 35% v/v H_2O_2 (0.22 mL) and a solution of $LiOH{\cdot}H_2O$ (1.32 mmol) in H_2O (1.5 mL). The reaction mixture was stirred at 0 °C for 6 h. THF was evaporated in vacuo and the aqueous phase was acidified with 6 N HCl and extracted with Et_2O. The combined organic layers were washed twice with brine, dried over Na_2SO_4, and evaporated to dryness affording the desired acids as white solids which were purified by recrystallization from suitable solvents.

4.16. Preparation of 28a and 30a (Scheme 6)

HCl (1 N, 6 mL) and glacial acetic acid (9 mL) were added to a suspension of commercially available D-(4-nitro) or (4-trifluoromethyl)phenylalanine (5 mmol) in H_2O (17 mL). The resulting solution was stirred and cooled to 0 °C and carefully added, during 0.5 h, of $NaNO_2$ (42 mmol) solution in H_2O (9 mL). The solution was stirred at rt for 22 h and carefully added, during 0.5 h, of concd HCl (5 mL). Water was distilled off and the residue was extracted six times with boiling acetone. Acetone was distilled off and the oily residue was dissolved in Et_2O and dried over Na_2SO_4. The solvent was evaporated to dryness affording the corresponding (*R*)-2-hydroxy-3-arylpropanoic acid as a pale yellow solid.[17] This solid was dissolved in abs EtOH (30 mL), added of two drops of concd H_2SO_4 and refluxed with stirring for 5 h. The solvent was removed under reduced pressure, the residue was dissolved in Et_2O and the resulting solution was washed twice with $NaHCO_3$ saturated solution and brine. After drying over Na_2SO_4, the evaporation of the solvent afforded the corresponding ethyl esters as white solids which were used in the next step without any further purification.

4.17. Preparation of ethyl (*S*)-2-(4-chloro-phenoxy)-3-(4-nitro or 4-trifluoromethyl-phenyl)propanoate (Scheme 6, Step c)

These compounds were prepared as reported in Scheme 1 for compounds **2b–4b** and **8b–10b** starting from **28a** or **30a** and 4-chloro-phenol in anhydrous toluene. The purification was carried out by column chromatography on silica gel using petroleum ether/ethyl acetate 98:2 as eluent.

4.18. (*S*)-Ethyl 2-(4-chloro-phenoxy)-3-(4-bromo-phenyl)propanoate (28b, Scheme 6)

(*S*)-Ethyl 2-(4-chloro-phenoxy)-3-(4-nitro-phenyl)propanoate (0.656 g, 2.0 mmol) was suspended in a mixture of 95% EtOH (20 mL) and glacial acetic acid (15 mL). The reaction mixture was stirred at rt for 0.5 h, afterward Fe (0.445 g, 7.96 mmol) was added and the resulting mixture was refluxed with stirring for 1.5 h. The mixture was poured into cooled to 0 °C saturated solution of K_2CO_3 and extracted four times with ethyl acetate. The collected organic phases were dried over Na_2SO_4 and evaporated to dryness affording a yellow oil (0.665 g). The desired (*S*)-ethyl 2-(4-chloro-phenoxy)-3-(4-amino-phenyl)propanoate (0.485 g, 76% yield) was obtained by column chromatography on silica gel (petroleum ether/ethyl acetate 85:15 as eluent), as a pale yellow oil which solidified on standing. GC/MS *m/z* (%): 321 (5) [M^++2], 319 (15) [M^+], 106 (100) [$C_7H_8N^+$]. This compound (0.485 g, 1.51 mmol) was suspended in 1.5 N HCl (4 mL) and the mixture was stirred and cooled to 0 °C for 0.5 h, then the suspension was carefully added, during 0.5 h, of $NaNO_2$ (0.155 g, 2.25 mmol) solution in H_2O (3 mL). The resulting mixture was stirred at 0 °C for 1 h and

then added to an heated to 36 °C solution of CuBr (0.649 g, 4.52 mmol) in 48% HBr (3 mL). The resulting solution was stirred at reflux for 2 h and at rt for 16 h. The mixture was poured into ice-water and extracted with Et_2O. The combined organic layers were washed twice with brine, dried over Na_2SO_4, and evaporated to dryness affording a brown solid, which was chromatographed on silica gel column (petroleum ether/ethyl acetate 95:5 as eluent) to obtain **28b** as a yellow solid (0.245 g, 43% yield). All the spectral data were in accordance with those reported for the ethyl ester of compound **22**.

4.19. Preparation of the ethyl esters of (*S*)-28 and (*S*)-29 (Scheme 6, Step f)

These compounds were prepared as reported for **6c** and **7c** starting from **28b** and phenyl- or 2-thiopheneboronic acid, K_2CO_3, and $Pd(Ph_3P)_4$ in anhydrous toluene at 95 °C. The purification was carried out by column chromatography on silica gel using petroleum ether/CH_2Cl_2 90:10 as eluent for the ethyl ester of **28** or petroleum ether/ethyl acetate 95:5 as eluent for the ethyl ester of **29**.

4.20. Preparation of (*R*)-28, (*R*)-29, and (*R*)-30

The first two compounds were prepared starting from the commercially available L-(4-iodo)phenylalanine according to Scheme 6 (Steps a, b, c, f, and g).

4.21. (*R*)-Ethyl 2-(4-chloro-phenoxy)-3-(4-iodo-phenyl)propanoate

Prepared as reported in Scheme 1 for compounds **2b–4b** and **8b–10b** starting from the compound above and 4-chloro-phenol in dry toluene.

4.22. Ethyl esters of (*R*)-28 and (*R*)-29

Prepared as reported for the ethyl esters of (*S*)-**28** or (*S*)-**29** starting from the compound above and phenyl- or 2-thiopheneboronic acid. 92% and 54% yields, respectively.

The final acids (*R*)-**28** and (*R*)-**29** were obtained as reported for the corresponding *S*-isomers.

4.23. Preparation of compound (*R*)-30

Compound (*R*)-**30** was synthesized as reported for (*S*)-**30** starting from the commercially available L-(4-trifluoromethyl)-phenylalanine.

5. Computational chemistry

Molecular modeling and graphics manipulations were performed using the molecular operating environment (MOE)[35] and UCSF CHIMERA software packages,[36] running on a Silicon Graphics Tezro R16000 workstation. Energy minimizations, MD simulations, and MM–PBSA calculations were realized by employing the AMBER 9 program,[37] selecting the parm99 force field.[38]

5.1. Ligand and receptor preparation

Model building and geometry optimizations of compounds (*S*)-**27**, (*S*)-**29**, and (*S*)-**30** were accomplished with the MMFF94X force field,[39–43] available within MOE. The carboxylate group was taken as dissociated. The crystal structures of hPPARα in complex with GW409544 (PDB code: 1K7L)[20] and hPPARγ in complex with rosiglitazone (PDB code: 2PRG)[21] were used in the docking experiments. Bound ligands and water molecules were removed. A correct atom assignment for Asn, Gln, and His residues was done, and hydrogen atoms were added using standard MOE geometries. Partial atomic charges were computed by MOE using the Amber99 force field. All heavy atoms were then fixed, and hydrogen atoms were minimized using the AMBER99 force field and a constant dielectric of 1, terminating at a gradient of 0.001 kcal mol^{-1} $Å^{-1}$.

5.2. Docking simulations

Compounds (*S*)-**27**, (*S*)-**29**, and (*S*)-**30** were docked into the active site of hPPARα and hPPARγ using the GOLD 3.1 program,[22,23] which uses a genetic algorithm for determining the docking modes of ligands and proteins. An advantage of GOLD over other docking methods is the program's ability to account for some rotational protein flexibility, as well as full ligand flexibility. Specifically, OH groups of Ser, Thr, and Tyr, and amino groups of Lys are allowed to rotate during docking to optimize H-bonding to the ligand. GOLD requires a user-defined binding site. It searches for a cavity within the defined area, and considers all the solvent-accessible atoms in that area as active-site atoms. The fitness score function implemented in GOLD (GOLDScore) is made up of four components that account for protein–ligand binding energy: protein-ligand H-bond energy (external H-bond), protein–ligand van der Waals energy (external vdw), ligand internal vdw energy (internal vdw), and ligand torsional strain energy (internal torsion). Parameters used in the fitness function (H-bond energies, atom radii, and polarizabilities, torsion potentials, H-bond directionalities, and so forth) are taken from the GOLD parameter file. The fitness score is taken as the negative of the sum of the energy terms, so larger fitness scores indicated better bindings. The fitness function has been optimized for the prediction of ligand binding positions rather than the prediction of binding affinities, although some correlation with the latter can be also found. The protein input file may be the entire protein structure or a part of it comprising only the residues that are in the region of the ligand binding site. In the present study, GOLD was allowed to calculate interaction energies within a sphere of a 13 Å radius centered on the OH oxygens of Y314 and Y473 in the hPPARα and hPPARγ structures, respectively. Fifty independent docking runs were performed for each docking experiment, using standard default settings with a population size of 100, a maximum number of 300,000 operations, and a mutation and crossover rate of 95. After docking, the best generated 10 solutions of each ligand were ranked according to their fitness scores calculated by the GOLDScore function.

5.3. MD Simulations

To eliminate any residual geometric strain, the obtained complexes were energy minimized for 5000 steps using combined steepest descent and conjugate gradient methods until a convergence value of 0.001 kcal mol^{-1} $Å^{-1}$. Upon minimization, the protein backbone atoms were held fixed. The geometry optimization was performed using the SANDER module in the AMBER suite of programs, employing the Cornell et al. force field to assign parameters for the standard amino acids. General AMBER force field (GAFF) parameters were assigned to ligands, while the partial charges were calculated using the AM1-BCC method as implemented in the ANTECHAMBER[44] suite of AMBER. The (*S*)-**27**/hPPARα complex was soaked in a box of TIP3P[45] water molecules with a margin of 10 Å along each dimension. An appropriate number of counterions were added to neutralize the system. The entire system was then minimized for 5000 steps using combined steepest descent and conjugate gradient methods until a convergence

value of 0.001 kcal mol^{-1} Å^{-1}. Upon minimization, harmonic constraints of 2 kcal mol^{-1} Å^{-2} on the protein backbone atoms of the complexes were applied. Such an energy-minimization was designed to resolve the clashes between the complex and solvent molecules gradually. The complex was then subjected to a three stage equilibration to further relax the protein and the surrounding solvent. In the first stage, the system was heated from 0 to 300 K (using the Langevin dynamics method) over 50 ps of simulation time. In the second stage, the system was equilibrated for 50 ps using pressure and temperature control to adjust the density of water to experimental values. In the third stage, a 500 ps of constant volume equilibration at 300 K was carried out. A subsequent production run was performed, giving a total simulation time of 3 ns. The time step of the simulations was 2.0 fs with a cutoff of 8 Å for the non-bonded interaction, and SHAKE[46] was employed to keep all bonds involving hydrogen atoms rigid.

5.4. Thermodynamic calculations

The method for determining the binding free energy following the MM–PBSA approach has been described in the past.[28–30] It combines molecular mechanics, Poisson–Boltzmann electrostatics, surface-accessible calculations, and normal mode analyses for the entropy. These are carried out on a series of snapshots collected from a MD simulation. The binding free energies (ΔG_{bind}) were computed as

$$\Delta G_{\text{bind}} = \Delta G(\text{complex}) - [\Delta G(\text{protein}) + \Delta G(\text{ligand})] \quad (1)$$

where ΔG(complex), ΔG(protein), and ΔG(ligand) are the free energies of the protein + ligand complex, the protein, and the ligand, respectively, averaged over a set of snapshots taken to represent the ensemble of available states. This set of snapshots is generated using MD.

With the MM–PBSA approach, the free energy for any single snapshot structure is given as

$$\Delta G_{\text{bind}} = \Delta E_{\text{gas}} + \Delta\Delta G_{\text{solv}} - T\Delta S \quad (2)$$

$$\Delta E_{\text{gas}} = \Delta E_{\text{int}} + \Delta E_{\text{ele}} + \Delta E_{\text{vdw}} \quad (3)$$

$$\Delta G_{\text{solv}} = \Delta G_{\text{PB}} + \Delta G_{\text{non-polar}} \quad (4)$$

The sum of molecular mechanical energies, ΔE_{gas}, can be divided into contributions from internal energy (ΔE_{int}), electrostatic potential (ΔE_{ele}), and van der Waals (ΔE_{vdw}) potential. The solvation free energy (ΔG_{solv}) is composed of two parts: polar solvation free energy (ΔG_{PB}) and non-polar solvation free energy ($\Delta G_{\text{non-polar}}$). $T\Delta S$ is the entropy contributions of the binding process.

From the resulting trajectories of the (*S*)-**27**/hPPARα complex, snapshots were extracted every 10 ps to use in calculating ΔE_{gas} and $\Delta\Delta G_{\text{solv}}$, giving 300 snapshots for the 3 ns runs. Solvent water was stripped off of these snapshots before they were used. The single trajectory approach was applied to estimate the energies. Estimation of energies in this manner has proven successful in many studies.[47–49] Part of the reason for the success of this approach is the cancelation of errors that hides the effect of incomplete sampling. A better approach may be the use of separate trajectories of protein–ligand complex, free protein, and free ligand. Unfortunately, due to sampling limitations, the separate trajectory approach appeared to be significantly less stable. ΔE_{gas} was obtained using SANDER, and estimation of ΔG_{PB} was conducted with the PBSA program in the AMBER suite, which numerically solves the Poisson–Boltzmann equations to determine the electrostatic contribution to the solvation free energy. Dielectric constants of 1 and 80 to represent gas and water phases, respectively, were applied. $\Delta G_{\text{nopolar}}$ was determined using the MOLSURF program, which is part of the AMBER suite of programs.

Acknowledgment

This work was accomplished thanks to the financial support of the Ministero dell'Istruzione, dell'Università e della Ricerca (MIUR 2005033023).

Supplementary data

Analytical data for intermediates and final compounds are given.

Supplementary data associated with this article can be found, in the online version, at doi:10.1016/j.bmc.2008.09.045.

References and notes

1. Zimmet, P. Z.; Alberti, K. G. M. M.; Shaw, J. *Nature* **2001**, *414*, 782.
2. Hulin, B. *Prog. Med. Chem.* **1994**, *31*, 1.
3. Moneva, M. H.; Dagogo-Jack, S. *Curr. Drug Targets* **2002**, *3*, 203.
4. Skyler, J. S. *J. Med. Chem.* **2004**, *47*, 4113. and references therein.
5. Nuclear Receptor Nomenclature Committee, *Cell* **1999**, *97*, 161.
6. Berger, J.; Moller, D. E. *Annu. Rev. Med.* **2002**, *53*, 409.
7. Krey, G.; Braissant, O.; L'Horset, F.; Kalkhoven, E.; Perroud, M.; Parker, M. G.; Wahli, W. *Mol. Endocrinol.* **1997**, *11*, 779.
8. Elisaf, M. *Curr. Med. Res. Opin.* **2002**, *18*, 269.
9. Barbier, O.; Torra, I. P.; Duguay, Y.; Blanquart, C.; Fruchart, J.-C.; Glineur, C.; Staels, B. *Arterioscler. Thromb. Vasc. Biol.* **2002**, *22*, 717.
10. Jiang, G.; Dallas-Yang, Q.; Li, Z.; Szalkowski, D.; Liu, F.; Shen, X.; Wu, M.; Zhou, G.; Doebber, T.; Berger, J.; Moller, D. E.; Zhang, B. B. *Diabetes* **2002**, *51*, 2412.
11. Picard, F.; Auwerx, J. *Annu. Rev. Nutr.* **2002**, *22*, 167.
12. Walter, H.; Lubben, G. *Drugs* **2005**, *65*, 1.
13. Gastaldelli, A.; Ferrannini, E.; Miyazaki, Y.; Matsuda, M.; Mari, A.; Defronzo, R. A. *Am. J. Physiol. Endocrinol. Metab.* **2007**, *292*, E871.
14. Pinelli, A.; Godio, C.; Laghezza, A.; Mitro, N.; Fracchiolla, G.; Tortorella, V.; Lavecchia, A.; Novellino, E.; Fruchart, J.-C.; Staels, B.; Crestani, M.; Loiodice, F. *J. Med. Chem.* **2005**, *48*, 5509.
15. Fracchiolla, G.; Laghezza, A.; Piemontese, L.; Carbonara, G.; Lavecchia, A.; Tortorella, P.; Crestani, M.; Novellino, E.; Loiodice, F. *ChemMedChem* **2007**, *2*, 641.
16. Carbonara, G.; Fracchiolla, G.; Loiodice, F.; Tortorella, P.; Conte-Camerino, D.; De Luca, A. M.; Liantonio, A. *Farmaco* **2001**, *56*, 749.
17. Winitz, M.; Bloch-Frankenthal, L.; Izumiya, N.; Birnbaum, S. M.; Baker, C. G.; Greenstein, J. P. *J. Am. Chem. Soc.* **1956**, *78*, 2423. and references therein.
18. Mitsunobu, O. *Synthesis* **1981**, 1.
19. Lehmann, J. M.; Moore, L. B.; Smith-Oliver, T. A.; Wilkison, W. O.; Willson, T. M.; Kliewer, S. A. *J. Biol. Chem.* **1995**, *270*, 12953.
20. Xu, H. E.; Lambert, M. H.; Montana, V. G.; Plunket, K. D.; Moore, L. B.; Collins, J. L.; Oplinger, J. A.; Kliewer, S. A.; Gampe, R. T., Jr.; McKee, D. D.; Moore, J. T.; Willson, T. M.; Stimmel, J. B. *Proc. Natl. Acad. Sci. U.S.A.* **2001**, *98*, 13919.
21. Nolte, R. T.; Wisely, G. B.; Westin, S.; Cobb, J. E.; Lambert, M. H.; Kurokawa, R.; Rosenfeld, M. G.; Willson, T. M.; Glass, C. K.; Milburn, M. V. *Nature* **1998**, *395*, 137.
22. GOLD 3.1. CCDC Software Limited: Cambridge, UK, 2007.
23. Jones, G.; Willett, P.; Glen, R. C.; Leach, A. R.; Taylor, R. J. *J. Mol. Biol.* **1997**, *267*, 727.
24. Schulz-Gasch, T.; Stahl, M. *J. Mol. Model.* **2003**, *9*, 47.
25. Wang, R.; Lu, Y.; Wang, S. *J. Med. Chem.* **2003**, *46*, 2287.
26. Kellenberger, E.; Rodrigo, J.; Muller, P.; Rognan, D. *Proteins: Struct. Funct. Bioinf.* **2004**, *57*, 225.
27. Warren, G. L.; Andrews, C. W.; Capelli, A. M.; Clarke, B.; LaLonde, J.; Lambert, M. H.; Lindvall, M.; Nevins, N.; Semus, S. F.; Senger, S.; Tedesco, G.; Wall, I. D.; Woolven, J. M.; Peishoff, C. E.; Head, M. S. *J. Med. Chem.* **2006**, *49*, 5912.
28. Srinivasan, J.; Cheatham, T. E., III; Cieplak, P.; Kollman, P. A.; Case, D. A. *J. Am. Chem. Soc.* **1998**, *120*, 9401.
29. Massova, I.; Kollman, P. A. *Perspect. Drug Discovery Des.* **2000**, *18*, 113.
30. Wang, W.; Lim, W. A.; Jakalian, A.; Wang, J.; Wang, J. M.; Luo, R.; Bayly, C. T.; Kollman, P. A. *J. Am. Chem. Soc.* **2001**, *123*, 3986.
31. Wang, J. M.; Morin, P.; Wang, W.; Kollman, P. A. *J. Am. Chem. Soc.* **2001**, *123*, 5221.
32. Lu, I. L.; Huang, C. F.; Peng, Y. H.; Lin, Y. T.; Hsieh, H. P.; Chen, C. T.; Lien, T. W.; Lee, H. J.; Mahindroo, N.; Prakash, E.; Yueh, A.; Chen, H. Y.; Goparaju, C. M.; Chen, X.; Liao, C. C.; Chao, Y. S.; Hsu, J. T.; Wu, S. Y. *J. Med. Chem.* **2006**, *49*, 2703.
33. Raspe, E.; Madsen, L.; Lefebvre, A.-M.; Leitersdorf, I.; Gelman, L.; Peinado-Onsurbe, J.; Dallongeville, J.; Fruchart, J.-C.; Berge, R.; Staels, B. *J. Lipid Res.* **1999**, *40*, 2099.
34. Hollons, T.; Yoshimura, F. K. *Anal. Biochem.* **1989**, *182*, 411.
35. Molecular Operating Environment (MOE), version 2005.06; Chemical Computing Group, Inc.: Montreal, Canada, 2005.
36. Huang, C. C.; Couch, G. S.; Pettersen, E. F.; Ferrin, T. E. *Pac. Symp. Biocomput.* **1996**, *1*, 724. http://www.cgl.ucsf.edu/chimera.
37. Case, D. A.; Darden, T. A.; Cheatham, T. E., III; Simmerling, C. L.; Wang, J.; Duke, R. E.; Luo, R.; Merz, K. M.; Wang, B.; Pearlman, D. A.; Crowley, M.; Brozell, S.;

Tsui, V.; Gohlke, H.; Mongan, J.; Hornak, V.; Cui, G.; Beroza, P.; Schafmeister, C.; Caldwell, J. W.; Ross, W. S.; Kollman, P. A. *AMBER*; University of California: San Francisco, 2006.
38. Cornell, W. D.; Cieplak, P.; Bayly, C. I.; Gould, I. R.; Merz, K. M., Jr.; Ferguson, D. M.; Spellmeyer, D. C.; Fox, T.; Caldwell, J. W.; Kollman, P. A. *J. Am. Chem. Soc.* **1995**, *117*, 5179.
39. Halgren, T. A. *J. Comput. Chem.* **1996**, *17*, 490.
40. Halgren, T. A. *J. Comput. Chem.* **1996**, *17*, 520.
41. Halgren, T. A. *J. Comput. Chem.* **1996**, *17*, 553.
42. Halgren, T. A. *J. Comput. Chem.* **1996**, *17*, 587.
43. Halgren, T. A. *J. Comput. Chem.* **1996**, *17*, 616.
44. Wang, J.; Wolf, R. M.; Caldwell, J. W.; Kollman, P. A.; Case, D. A. *J. Comput. Chem.* **2004**, *25*, 1157.
45. Jorgensen, W. L.; Chandrasekhar, J.; Madura, J. D.; Impey, R. W.; Klein, M. L. *J. Chem. Phys.* **1983**, *79*, 926.
46. Ryckaert, J. P.; Ciccotti, G.; Berendsen, H. J. C. *J. Comput. Phys.* **1977**, *23*, 327.
47. Zhuang, S. L.; Zou, J. W.; Jiang, Y. J.; Mao, X.; Zhang, B.; Liu, H. C.; Yu, Q. S. *J. Med. Chem.* **2005**, *48*, 7208.
48. Bao, J.; Zhang, D. W.; Zhang, J. Z. H.; Lee Huang, P.; Lin Huang, P.; Lee-Huang, S. *FEBS Lett.* **2007**, *581*, 2737.
49. Hou, T. J.; Guo, S. L.; Xu, X. J. *J. Phys. Chem. B* **2002**, *106*, 5527.